

Supplementary Information

Nanoconfined Carbonization Enabling High-Density Porous Carbon for Jointly Superior Gravimetric and Volumetric Zinc-Ion Storage

Jiacong Lu^a, Xinyue Zhong^a, Xiaomin Lin^a, Jiuqing Gui^a, Mingtao Zheng^{ab}, Yingliang Liu^a, Yeru Liang^{*ab}

^a*Key Laboratory for Biobased Materials and Energy of Ministry of Education, College of Materials and Energy, South China Agricultural University, Guangzhou 510642, P. R. China*

^b*Maoming Branch, Guangdong Laboratory of Lingnan Modern Agriculture, Maoming 525000, P. R. China*

Experimental Section

Materials

Glucose was purchased from Shanghai RichJoint Chemical Reagents Co., Ltd.. Urea and ZnSO₄·7H₂O were purchased from Shanghai Aladdin Biochemical Technology Co.,Ltd.. Tetraethyl orthosilicate (TEOS) was purchased from Tianjin Luck Early morning Chemistry Reagent plant. 98wt% H₂SO₄ and 40wt% Hydrofluoric acid were purchased from Guangzhou Chemical Reagent Co., Ltd.. All chemicals were analytical grade and used as received.

Preparation of LCC

0.9 g of glucose and 0.6 g of urea were dissolved in 1.5 mL of pH 2.0 H₂SO₄ aqueous solution under stirring until clear. The resulting mixture was placed in an open flask at 40 °C for 2 days, followed by vacuum drying at 60 °C for 1 day, and subsequent drying at 100 °C and 160 °C for 6 h each. The sample was then carbonized up to 700 °C with a heating rate of 5 °C min⁻¹ in N₂ flow for 2 h. After carbonization, the resulting sample was filtered, dried, and denoted as LCC.

Preparation of HDPCs

0.9 g of glucose and 0.6 g of urea were dissolved in 1.5 mL of pH 2.0 H₂SO₄ aqueous solution under stirring until clear. Subsequently, x mL of tetraethyl orthosilicate (TEOS) was added with continuous stirring until homogenization. The resulting mixture was aged in an open flask at 40 °C for 2 days, followed by vacuum drying at 60 °C for 1 day, and subsequent drying at 100 °C and 160 °C for 6 h each. The samples were then carbonized up to 700 °C with a heating rate of 5 °C min⁻¹ in N₂ flow for 2 h. After carbonization, the black carbon/silica nanocomposite underwent washing with 40 wt% hydrofluoric acid to remove the silica, followed by filtration, drying, and denoted as HDPC-x.

Preparation of LCC, HDPCs and YP-50F electrodes

LCC, HDPCs, and YP-50F electrodes were prepared by mixing LCC, HDPC-x, and YP-50F, respectively, with acetylene black and poly(vinylidene fluoride) binder at a

weight ratio of 8:1:1 in 1-methyl-2-pyrrolidinone. The slurry was pasted on carbon paper and dried overnight at 80 °C. The electrodes have a diameter of 12 mm, corresponding to an approximate area of 113 mm². Typically, the mass loadings of all cathodes are maintained at 1-1.5 mg cm⁻². To assess the electrochemical performance of the samples under higher mass loadings, the cathode mass loadings were varied from 4.2 mg cm⁻² to 12.5 mg cm⁻².

Materials Characterization

The microstructures of prepared samples were characterized using high-resolution transmission electron microscopy (Talos F200S, FEI) and scanning electron microscopy (SU8220, Hitachi). Thermogravimetric analysis was performed using a thermal gravimetric analyzer (TG209F1LibraTM, NETZSCH) from room temperature to 700 °C at a rate of 5 °C min⁻¹ in N₂, and from room temperature to 900 °C at a rate of 10 °C min⁻¹ in air. X-ray powder diffraction patterns were obtained with an X-ray diffraction meter (Ultima IV, Rigaku) using Cu/K- α radiation at a scanning rate of 10°min⁻¹ from 10° to 80° ($\lambda = 0.15418$ nm). Density was assessed using a Tap Density Tester (FT-100A, Rlco) with a vibration frequency of 180 times per minute. Pore structure parameters were determined using an ASAP 3Flex automatic volumetric sorption analyzer at 77 K (Micromeritics Sorption Analyzer). Specific surface area (S_{BET}) was analyzed by Brunauer-Emmett-Teller theory, and micropore surface area (S_{micro}) was determined using the t-plot method. The pore size distribution was analyzed by original density functional theory (DFT) combined with non-negative regularization and medium smoothing.

Electrochemical Measurements

The aqueous zinc-ion hybrid supercapacitors (ZHSCs) were assembled in 2025 coin-type cell with the as-prepared carbon electrode as cathode, Zn foil as anode and 2M ZnSO₄ as electrolyte. Galvanostatic charge-discharge tests were conducted using a Neware battery cycler (CT4008-5V10mA-164) over a voltage range of 0-1.8 V at various current densities. Electrochemical impedance spectroscopy was performed on a Modulab XM DSSC with an amplitude of 5 mV over a frequency range from 100

kHz to 10 mHz. Cyclic voltammetry tests were conducted using a CHI660E electrochemical workstation, with voltage scanning from 0 to 1.8 V at scanning rates of 5, 10, 20, 50, and 100 mV s⁻¹. Ex-situ X-ray diffraction analysis of electrodes commenced with assembly into zinc-ion hybrid supercapacitor coin cells, followed by constant current charge-discharge cycling to a predetermined voltage. Subsequently, the cell was disassembled, and the electrode was meticulously cleaned, and dried for one day. The prepared electrodes were then subjected to X-ray diffraction analysis using an Ultima IV diffractometer (Rigaku) with Cu/K- α radiation at a scanning rate of 10° min⁻¹ over a range of 10° to 80° ($\lambda = 0.15418$ nm). Gravimetric capacitance (C_g , F g⁻¹) and volumetric capacitance (C_v , F cm⁻³) of carbon cathode were calculated from galvanostatic charge-discharge curves using Equations (1) and (2), respectively:¹

$$C_g = \frac{I \Delta t}{m \Delta U} \quad (1)$$

$$C_v = C_g \times \rho \quad (2)$$

where I is the current density, Δt is the discharging time, m is the mass loading, ΔU is the discharge voltage, and ρ is the density. Gravimetric energy density (E_g , Wh kg⁻¹) and volumetric energy density (E_v , Wh L⁻¹) were calculated by Equations (3) and (4), respectively:¹

$$E_g = \frac{C_g (\Delta U)^2}{2 \times 3.6} \quad (3)$$

$$E_v = E_g \times \rho \quad (4)$$

The corresponding gravimetric (P_g , W kg⁻¹) and volumetric power density (P_v , W L⁻¹) were obtained from Equations (5) and (6), respectively:¹

$$P_g = \frac{3600 \times E_g}{\Delta t} \quad (5)$$

$$P_v = P_g \times \rho \quad (6)$$

Capacitance per surface area (C_s , F m⁻²) of carbon cathode were calculated using Equations (7):²

$$C_s = \frac{C_g}{S} \quad (7)$$

where S is the SSA. Notably, $C_{s,>x \text{ nm}}$ and $C_{s,y-z \text{ nm}}$ represent C_s of pores with diameters exceeding x nm and ranging from y nm to z nm, respectively.

Relative standard deviation (RSD) were calculated by Equations (8):

$$\text{RSD} = \frac{s}{\bar{x}} \times 100\% = \sqrt{\frac{\sum_{i=1}^n (x_i - \bar{x})^2}{n-1}} \times \frac{1}{\bar{x}} \times 100\% \quad (8)$$

where s is the standard deviation and \bar{x} is the average.

Supplementary Figures



Fig. S1 Digital photo of carbon/silica composite.

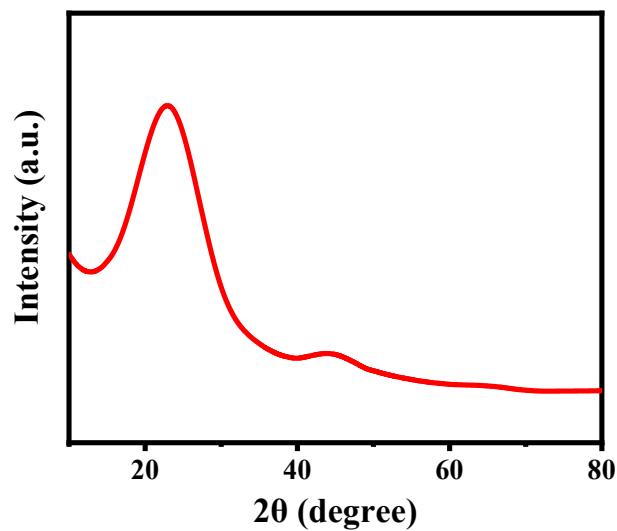


Fig. S2 XRD pattern of the carbon/silica composite for preparing HDPC-1.

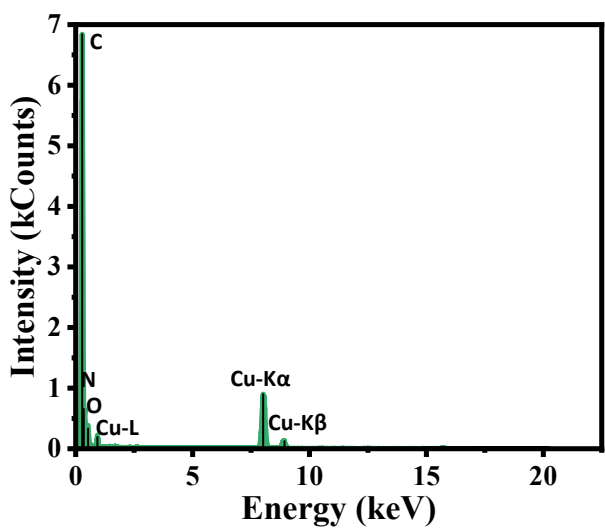


Fig. S3 Energy dispersive X-ray spectroscopic analyses from TEM observation for HDPC-1.

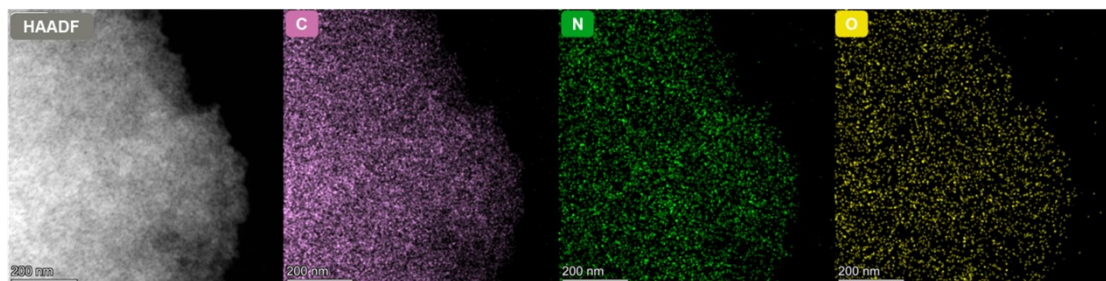


Fig. S4 Electron energy loss spectroscopy mapping images of HDPC-1.

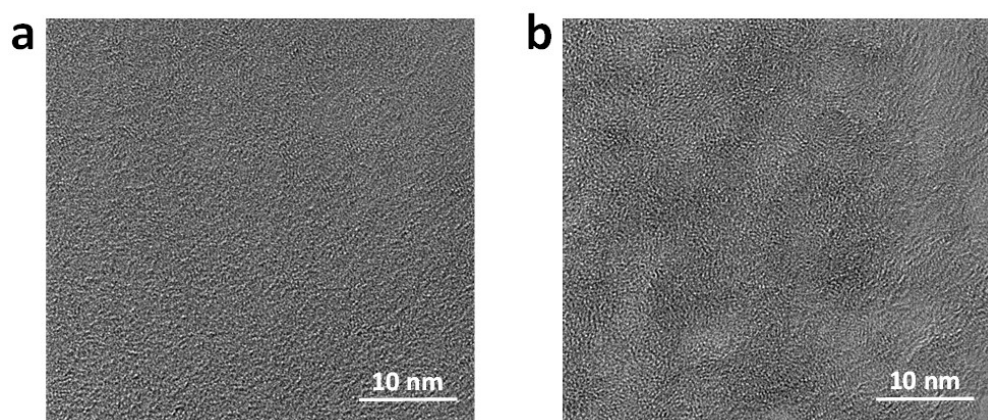


Fig. S5 High-resolution TEM images of (a) LCC and (b) HDPC-1.

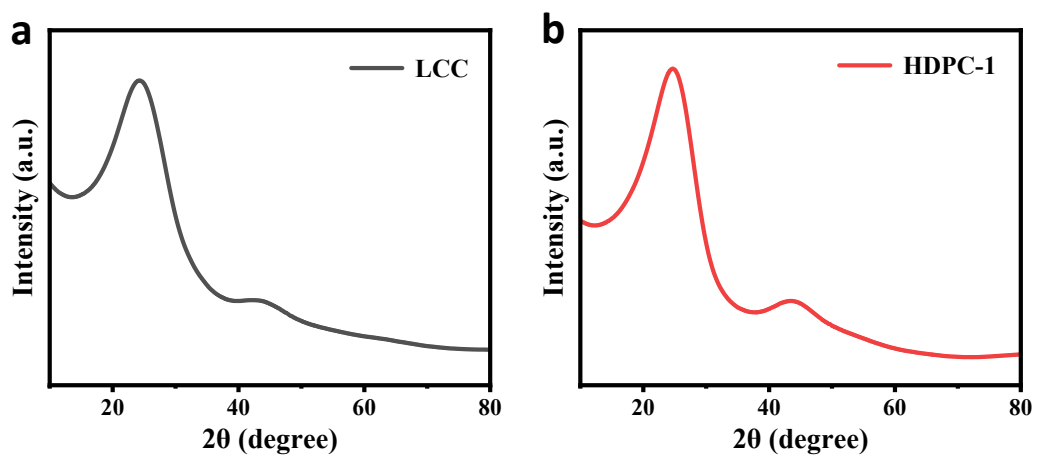


Fig. S6 XRD patterns of (a) LCC and (b) HDPC-1.

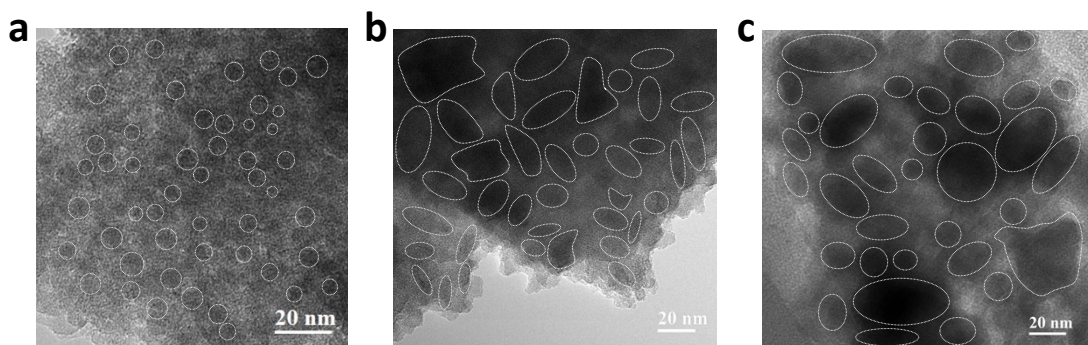


Fig. S7 TEM images of the carbon/silica composites for preparing (a) HDPC-1, (b) HDPC-2 and (c) HDPC-3. Dashed circles indicate the silica components within the composites.

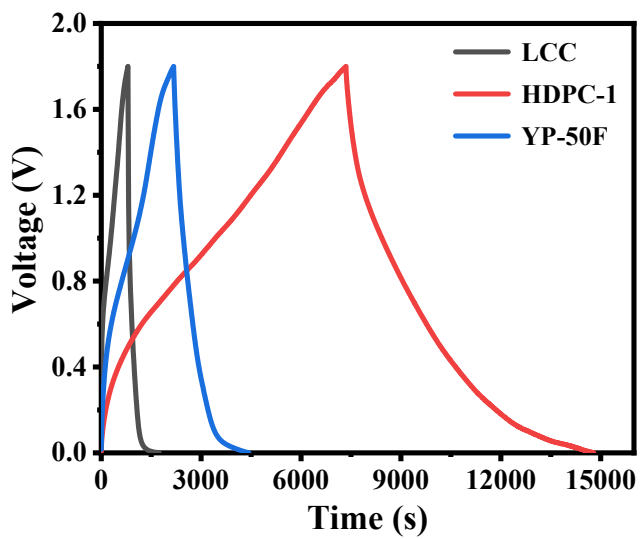


Fig. S8 Galvanostatic charge-discharge curves of LCC, HDPC-1 and YP-50F at a current density of 0.1 A g^{-1} .

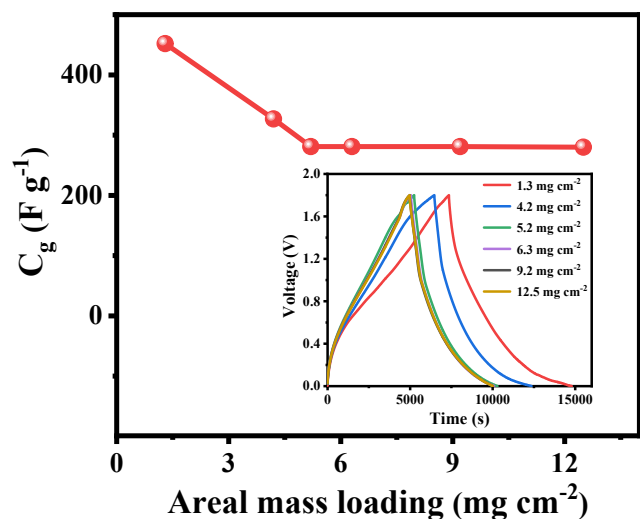


Fig. S9 C_g of HDPC-1 under various areal mass loadings.

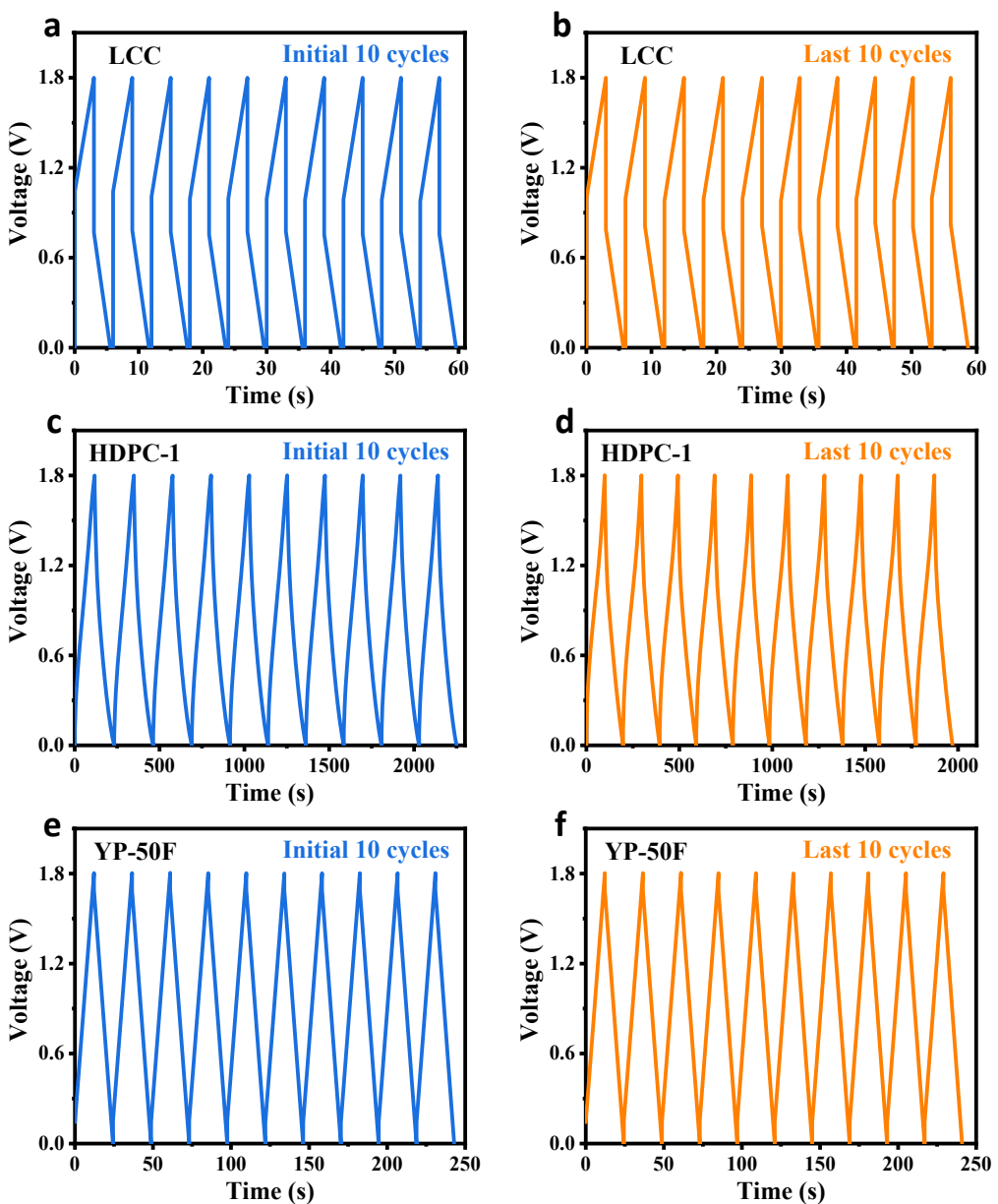


Fig. S10 Galvanostatic charge-discharge curves for the initial ten cycles and last ten cycles of the (a, b) LCC, (c, d) HDPC-1 and (e, f) YP-50F at 5 A g^{-1} .

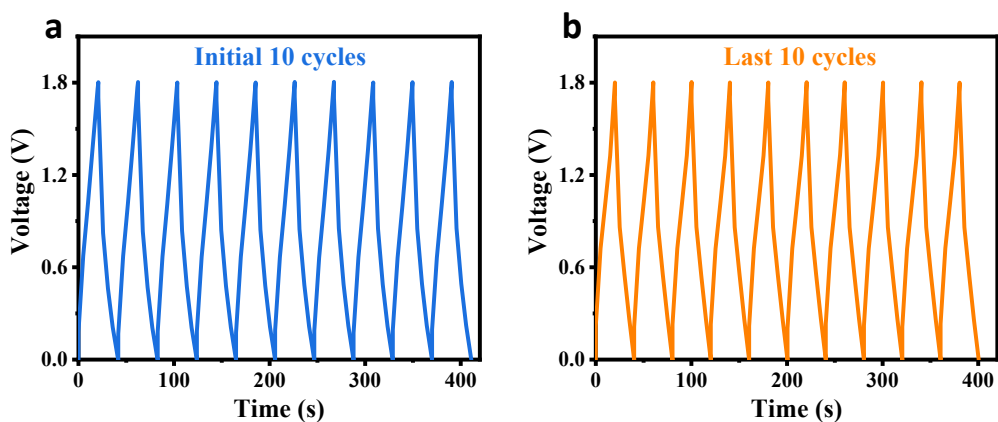


Fig. S11 Galvanostatic charge-discharge curves for the (a) initial ten cycles and (b) last ten cycles of the HDPC-1 at 20 A g^{-1} .

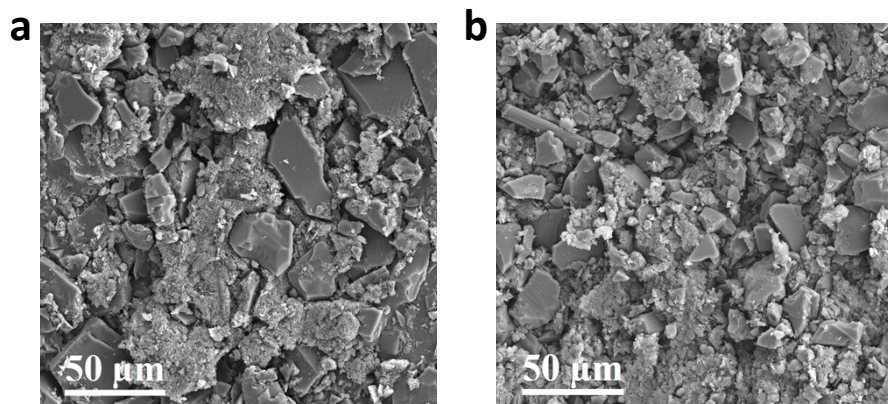


Fig S12. SEM images of the HDPC-1 cathodes (a) before cycling and (b) after 300000 cycles at 20 A g^{-1} .

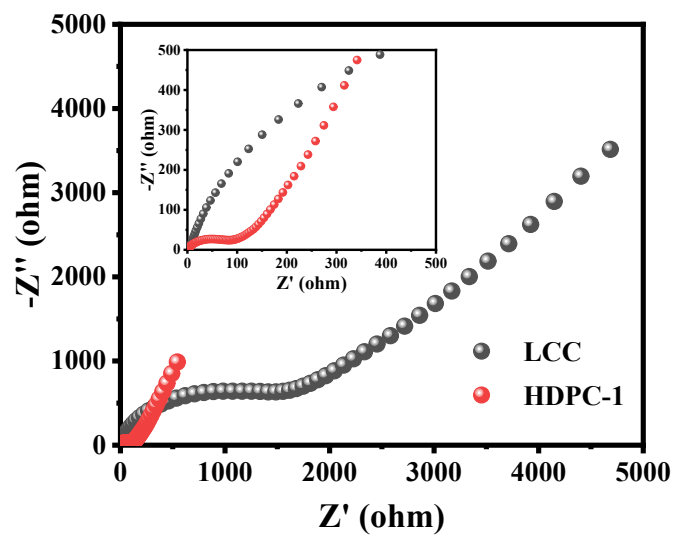


Fig. S13 Nyquist plots of LCC and HDPC-1.

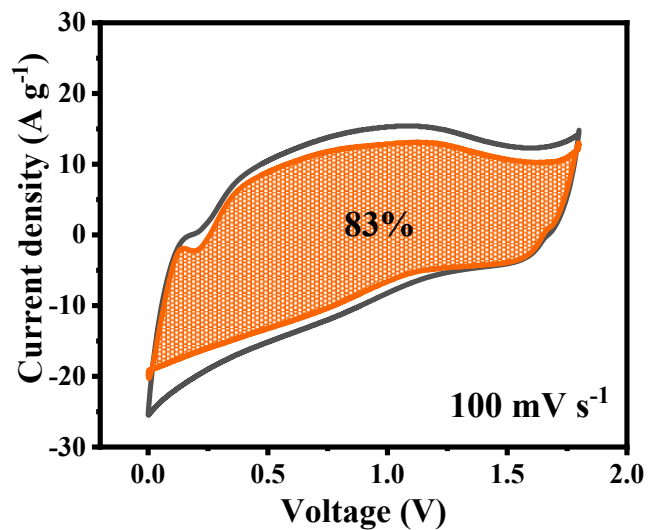


Fig. S14 Capacitive contribution at 100 mV s^{-1} of HDPC-1.

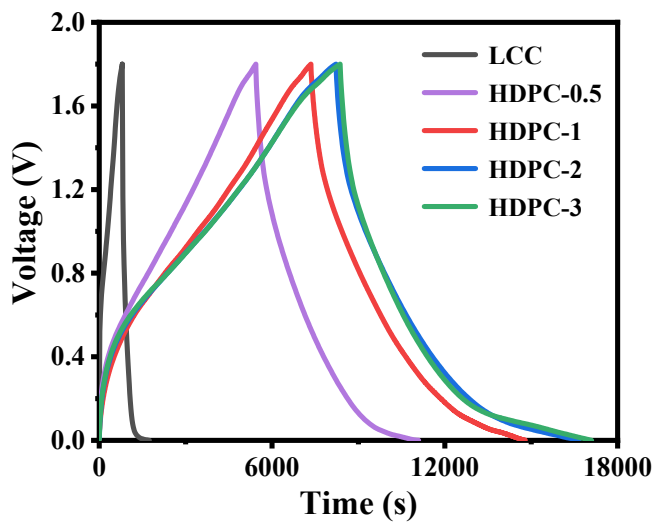


Fig. S15 Galvanostatic charge-discharge curves of LCC and HDPCs at a current density of 0.1 A g^{-1} .

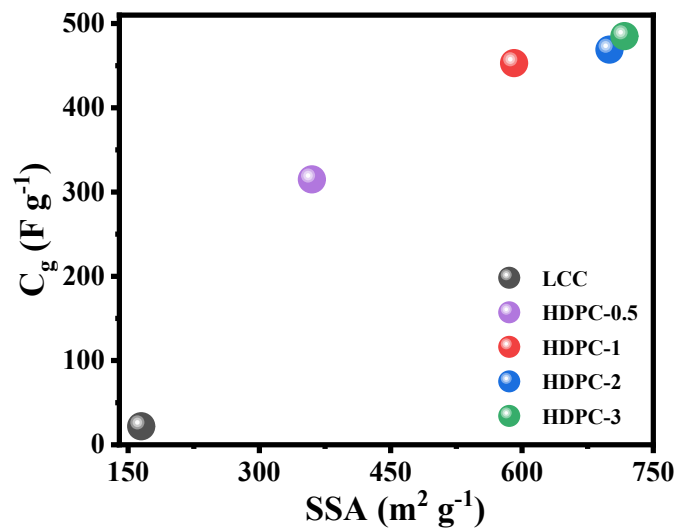


Fig. S16 Absence of direct correlation between C_g and SSA in LCC and HDPCs.

Supplementary Tables

Table S1 Comparison of ρ between HDPC-1 and other carbon materials.

Sample	ρ (g cm^{-3})	SSA ($\text{m}^2 \text{ g}^{-1}$)	Reference
HGF	0.71	830	3
CDC	0.53	1202	4
PF16G-HA	0.40	3523	5
Compressed-25	0.75	707	6
asMEG-O	0.59	3290	7
AQSGH	0.05	1050	8
CXA η -30	0.66	1133	9
SP4-3	0.49	2335	10
AC500	0.51	2074	11
RAC-800-2	0.55	1911	12
HDPC-1	0.78	591	This work

Table S2 Pore structure and ρ of LCC and HDPCs.

Sample	S_{BET} ($\text{m}^2 \text{ g}^{-1}$)	S_{micro} ($\text{m}^2 \text{ g}^{-1}$)	V_{total} ($\text{cm}^3 \text{ g}^{-1}$)	V_{micro} ($\text{cm}^3 \text{ g}^{-1}$)	ρ (g cm^{-3})
LCC	165	165	0.06	0.05	0.22
HDPC-0.5	360	264	0.32	0.09	0.92
HDPC-1	591	393	0.61	0.14	0.78
HDPC-2	700	384	1.30	0.06	0.32
HDPC-3	717	388	1.41	0.03	0.15

Table S3 Comparison of C_g between HDPC-1 with reported carbon-based materials for ZHSCs under various areal mass loadings.

Sample	Mass loading (mg cm ⁻²)	Current density (A g ⁻¹)	C_g (F g ⁻¹ /mAh g ⁻¹)	Reference
PSC-A600	2	0.2	413.3 F g ⁻¹	13
N,P-OLC	0.5	0.5	420.3 F g ⁻¹	14
Zn-3-MnO ₂	2-3	0.2	282.9 F g ⁻¹	15
75%NHG-rGO	0.66	0.1	198 F g ⁻¹	16
NMCSs	1-1.2	0.2	355 F g ⁻¹	17
3D-PG-1	1	0.1	217 F g ⁻¹	18
DFs	1.6	0.2	35.1 F g ⁻¹	19
HOGS	2	0.1	175 F g ⁻¹	20
HOGS	10	0.1	200 F g ⁻¹	20
N-HPLC-700	3	0.2	354 F g ⁻¹	21
FCNSs	2	0.2	198 F g ⁻¹	22
S-3DPC-800	5	0.5	168.2 mAh g ⁻¹	23
ANHPC-2	1	0.5	197.2 mAh g ⁻¹	24
ANHPC-2	10	0.5	103.4 mAh g ⁻¹	24
PCNF-4	1.2	0.5	177 mAh g ⁻¹	25
BN-C	1	0.1	190.2 mAh g ⁻¹	26
HPC-CC	1.5-2	0.5	138.5 mAh g ⁻¹	27
PPy/N-rGO	1-1.2	0.1	145.3 mAh g ⁻¹	28
R6	1	0.5	168.4 mAh g ⁻¹	29
PHCA	2	1	143.7 mAh g ⁻¹	30
AC	0.7-0.8	0.1	121 mAh g ⁻¹	31
NPC	1.5	0.2	136.2 mAh g ⁻¹	32
N/P/O-PC-1200	5	0.2	125.3 mAh g ⁻¹	33

Sample	Mass loading (mg cm ⁻²)	Current density (A g ⁻¹)	C _g (F g ⁻¹ /mAh g ⁻¹)	Reference
ZnHPC-0.5	2	0.5	120.3 mAh g ⁻¹	34
PANI	1.5	0.05	200 mAh g ⁻¹	35
HDPC-1	1.3	0.1	452 F g⁻¹/227 mAh g⁻¹	This work
HDPC-1	12.5	0.1	280 F g⁻¹/140 mAh g⁻¹	This work

Table S4 Comparison of E_g and P_g between HDPC-1 and other carbon-based materials for ZHSCs.

Sample	P_g (W kg^{-1})	E_g (Wh kg^{-1})	Reference
NS-OPC	6063	53	36
RNP-1-2-Air	4000	54	37
NPG-0.75	4500	94	38
75%NHG-rGO	3750	57	16
NMCSs	160	126	17
OPC	3760	38	39
MXene-rGO2	279	34	40
Kelp-carbon	1300	111	41
C2NN1-800-1-5	180	133	42
HOPC	4000	71	43
FCNSs	39333	41	22
S-3DPC-800	160	162	23
DGH	400	78	44
N-CNF	367	143	45
3D-PG-1	85	86	27
YP-50F	90	42	This work
HDPC-1	45000	68	This work

Table S5 Comparison of E_v and P_v between HDPC-1 and other carbon-based materials for ZHSCs.

Sample	P_v (W L^{-1})	E_v (Wh L^{-1})	Reference
NP-CNC	9100	82	1
75%NHG-rGO	3750	58	16
NMCSs	40	32	17
FCNSs	17700	19	22
S-3DPC-800	97	99	23
DGH	600	118	44
3D-PG-1	116	118	27
YP-50F	36	17	This work
HDPC-1	35100	53	This work

Table S6 Electrochemical impedance spectroscopy parameters of LCC and HDPC-1 cathodes.

Sample	Ohmic resistance R_s (Ω)	Charge transfer resistance R_{ct} (Ω)
LCC	2.3	1864.0
HDPC-1	1.3	81.1

Table S7 C_g of LCC and HDPCs at various current densities.

Sample	0.1 A g ⁻¹ (F g ⁻¹)	0.2 A g ⁻¹ (F g ⁻¹)	0.5 A g ⁻¹ (F g ⁻¹)	1 A g ⁻¹ (F g ⁻¹)	2 A g ⁻¹ (F g ⁻¹)	5 A g ⁻¹ (F g ⁻¹)	10 A g ⁻¹ (F g ⁻¹)	20 A g ⁻¹ (F g ⁻¹)	50 A g ⁻¹ (F g ⁻¹)
LCC	22	14	8	6	5	4.5	4.4	4.2	4.1
HDPC-0.5	315	220	166	136	115	95	82	73	57
HDPC-1	453	382	332	309	281	255	235	212	151
HDPC-2	469	410	362	349	322	282	252	225	176
HDPC-3	485	422	376	361	340	306	276	240	192

Table S8 C, N, and H content from elemental analysis of LCC and HDPCs.

Sample	C (wt.%)	N (wt.%)	H (wt.%)
LCC	73.52	12.81	2.36
HDPC-0.5	73.25	13.94	1.92
HDPC-1	74.04	13.05	2.03
HDPC-2	73.28	13.63	2.12
HDPC-3	72.56	13.51	2.19

Table S9 C_s of different pore size subsections of LCC and HDPCs for the identification of the lower threshold value.

Sample	$C_{s,>0.55\text{ nm}}$ (F m ⁻²)	$C_{s,>0.6\text{ nm}}$ (F m ⁻²)	$C_{s,>0.7\text{ nm}}$ (F m ⁻²)	$C_{s,>0.8\text{ nm}}$ (F m ⁻²)	$C_{s,>0.9\text{ nm}}$ (F m ⁻²)	$C_{s,>1.0\text{ nm}}$ (F m ⁻²)	$C_{s,>1.1\text{ nm}}$ (F m ⁻²)	$C_{s,>1.2\text{ nm}}$ (F m ⁻²)	$C_{s,>1.3\text{ nm}}$ (F m ⁻²)
LCC	0.26	0.26	0.35	0.48	0.48	0.54	1.10	3.67	4.40
HDPC-0.5	1.29	1.45	1.93	2.42	2.58	2.60	2.69	2.89	3.18
HDPC-1	1.14	1.24	1.54	1.89	2.15	2.22	2.28	2.34	2.42
HDPC-2	1.16	1.28	1.58	1.75	1.76	1.76	1.76	1.84	1.91
HDPC-3	1.25	1.37	1.61	1.72	1.72	1.72	1.72	1.80	1.82

Note: $C_{s,>0.55\text{ nm}}$, $C_{s,>0.6\text{ nm}}$, $C_{s,>0.7\text{ nm}}$, $C_{s,>0.8\text{ nm}}$, $C_{s,>0.9\text{ nm}}$, $C_{s,>1.0\text{ nm}}$, $C_{s,>1.1\text{ nm}}$, $C_{s,>1.2\text{ nm}}$, and $C_{s,>1.3\text{ nm}}$ represent C_s of pores with diameters above 0.55 nm, above 0.6 nm, above 0.7 nm, above 0.8 nm, above 0.9 nm, above 1.0 nm, above 1.1 nm, above 1.2 nm, and above 1.3 nm, respectively.

Table S10 RSD of C_s for different pore size subsections to determine the lower threshold value.

C_s	$C_{s,>0.55\text{ nm}}$	$C_{s,>0.6\text{ nm}}$	$C_{s,>0.7\text{ nm}}$	$C_{s,>0.8\text{ nm}}$	$C_{s,>0.9\text{ nm}}$	$C_{s,>1.0\text{ nm}}$	$C_{s,>1.1\text{ nm}}$	$C_{s,>1.2\text{ nm}}$	$C_{s,>1.3\text{ nm}}$
RSD	0.4203	0.4345	0.4322	0.4326	0.4522	0.4402	0.3162	0.3137	0.3906

Table S11 C_s of different pore size subsections of LCC and HDPCs for the identification of the upper threshold value.

Sample	$C_{s,1.2-2 \text{ nm}}$ (F m ⁻²)	$C_{s,1.2-3 \text{ nm}}$ (F m ⁻²)	$C_{s,1.2-4 \text{ nm}}$ (F m ⁻²)	$C_{s,1.2-5 \text{ nm}}$ (F m ⁻²)	$C_{s,1.2-5.5 \text{ nm}}$ (F m ⁻²)	$C_{s,1.2-6 \text{ nm}}$ (F m ⁻²)	$C_{s,1.2-7 \text{ nm}}$ (F m ⁻²)	$C_{s,1.2-8 \text{ nm}}$ (F m ⁻²)
LCC	3.67	3.67	3.67	3.67	3.67	3.67	3.67	3.67
HDPC-0.5	10.16	8.75	7.16	5.00	3.66	3.25	2.89	2.86
HDPC-1	13.32	10.53	8.24	5.27	3.46	2.92	2.46	2.40
HDPC-2	13.03	12.68	10.20	6.09	3.97	3.37	2.88	2.71
HDPC-3	10.32	9.70	7.82	5.51	4.08	3.59	3.01	2.77

Note: $C_{s,1.2-2 \text{ nm}}$, $C_{s,1.2-3 \text{ nm}}$, $C_{s,1.2-4 \text{ nm}}$, $C_{s,1.2-5 \text{ nm}}$, $C_{s,1.2-5.5 \text{ nm}}$, $C_{s,1.2-6 \text{ nm}}$, $C_{s,1.2-7 \text{ nm}}$, and $C_{s,1.2-8 \text{ nm}}$ represent C_s of pores with diameters from 1.2 nm to 2 nm, from 1.2 nm to 3 nm, from 1.2 nm to 4 nm, from 1.2 nm to 5 nm, from 1.2 nm to 5.5 nm, from 1.2 nm to 6 nm, from 1.2 nm to 7 nm, and from 1.2 nm to 8 nm, respectively.

Table S12 RSD of C_s for different pore size subsections to determine the upper threshold value.

C_s	$C_{s,1.2-2}$	$C_{s,1.2-3}$	$C_{s,1.2-4}$	$C_{s,1.2-5}$	$C_{s,1.2-5.5}$	$C_{s,1.2-6}$	$C_{s,1.2-7}$	$C_{s,1.2-8}$
	nm	nm	nm	nm	nm	nm	nm	nm
RSD	0.3848	0.3693	0.3211	0.1763	0.0669	0.0883	0.1461	0.1639

Table S13 Capacitance retention (CR) for LCC and HDPCs across current densities from 0.1 A g^{-1} to various values.

Sample	CR _{0.1-0.2} (%)	CR _{0.1-0.5} (%)	CR _{0.1-1} (%)	CR _{0.1-2} (%)	CR _{0.1-5} (%)	CR _{0.1-10} (%)	CR _{0.1-20} (%)	CR _{0.1-50} (%)
LCC	64	36	27	23	21	20	19	18
HDPC-0.5	70	53	43	37	30	26	23	18
HDPC-1	84	73	68	62	56	52	46	33
HDPC-2	87	77	74	69	60	54	48	38
HDPC-3	87	78	75	70	63	57	50	40

Note: CR_{0.1-0.2}, CR_{0.1-0.5}, CR_{0.1-1}, CR_{0.1-2}, CR_{0.1-5}, CR_{0.1-10}, CR_{0.1-20}, and CR_{0.1-50} represent CR from 0.1 A g^{-1} to 0.2 A g^{-1} , from 0.1 A g^{-1} to 0.5 A g^{-1} , from 0.1 A g^{-1} to 1 A g^{-1} , from 0.1 A g^{-1} to 2 A g^{-1} , from 0.1 A g^{-1} to 5 A g^{-1} , from 0.1 A g^{-1} to 10 A g^{-1} , from 0.1 A g^{-1} to 20 A g^{-1} , and from 0.1 A g^{-1} to 50 A g^{-1} , respectively.

Supplementary References

- 1 L. Yang, X. He, Y. Wei, H. Bi, F. Wei, H. Li, C. Yuan and J. Qiu, *Nano Research*, 2022, **15**, 4068.
- 2 J. Wang, X. Yang, D. Wu, R. Fu, M. Dresselhaus and G. Dresselhaus, *Journal of Power Sources*, 2008, **185**, 589.
- 3 Y. Xu, Z. Lin, X. Zhong, X. Huang, N. Weiss, Y. Huang and X. Duan, *Nature Communications*, 2014, **5**, 4554.
- 4 C. Largeot, C. Portet, J. Chmiola, P. Taberna, Y. Gogotsi and P. Simon, *Journal of the American Chemical Society*, 2008, **130**, 2730.
- 5 L. Zhang, F. Zhang, X. Yang, G. Long, Y. Wu, T. Zhang, K. Leng, Y. Huang, Y. Ma, A. Yu and Y. Chen, *Scientific Reports*, 2013, **3**, 1408.
- 6 S. Murali, N. Quarles, L. Zhang, J. Potts, Z. Tan, Y. Lu, Y. Zhu and R. Ruoff, *Nano Energy*, 2013, **2**, 764.
- 7 T. Kim, G. Jung, S. Yoo, K. Suh and R. Ruoff, *ACS Nano*, 2013, **7**, 6899.
- 8 Q. Wu, Y. Sun, H. Bai and G. Shi, *Physical Chemistry Chemical Physics*, 2011, **13**, 11193.
- 9 Z. Zapata-Benabithe, F. Carrasco-Marín, J. Vicente and C. Moreno-Castilla, *Langmuir*, 2013, **29**, 6166.
- 10 A. Alonso, V. Ruiz, C. Blanco, R. Santamaría, M. Granda, R. Menéndez and S. Jager, *Carbon*, 2006, **44**, 441.
- 11 B. Xu, Y. Chen, G. Wei, G. Cao, H. Zhang and Y. Yang, *Materials Chemistry and Physics*, 2010, **124**, 504.
- 12 C. Zhao, Y. Huang, C. Zhao, X. Shao and Z. Zhu, *Electrochimica Acta*, 2018, **291**, 287.
- 13 Z. Li, D. Chen, Y. An, C. Chen, L. Wu, Z. Chen, Y. Sun and X. Zhang, *Energy Storage Materials*, 2020, **28**, 307.
- 14 H. Wang, Q. Chen, P. Xiao and L. Cao, *ACS Applied Materials & Interfaces*, 2022, **14**, 9013.
- 15 S. He, Z. Mo, C. Shuai, W. Liu, R. Yue, G. Liu, H. Pei, Y. Chen, N. Liu and R. Guo,

Applied Surface Science, 2022, **577**, 151904.

- 16 J. Luo, L. Xu, H. Liu, Y. Wang, Q. Wang, Y. Shao, M. Wang, D. Yang, S. Li, L. Zhang, Z. Xia, T. Cheng and Y. Shao, *Advanced Functional Materials*, 2022, **32**, 2112151.
- 17 Z. Peng, J. Guo, Q. He, S. Li, L. Tan and Y. Chen, *Sci. China Mater.*, 2022, **65**, 2401.
- 18 X. Xu, X. Zhao, Z. Yang, Q. Lin, B. Jian, N. Li, C. Zheng and W. Lv, *Carbon*, 2022, **186**, 624.
- 19 Z. Jian, N. Yang, M. Vogel, S. Leith, A. Schulte, H. Schönherr, T. Jiao, W. Zhang, J. Müller, B. Butz and X. Jiang, *Advanced Energy Materials*, 2020, **10**, 2002202.
- 20 H. Ma, H. Geng, B. Yao, M. Wu, C. Li, M. Zhang, F. Chi and L. Qu, *ACS Nano*, 2019, **13**, 9161.
- 21 F. Fu, D. Yang, Y. Fan, X. Qiu, J. Huang, Z. Li and W. Zhang, *Journal of Colloid and Interface Science*, 2022, **628**, 90.
- 22 H. Zhou, C. Liu, J. Wu, M. Liu, D. Zhang, H. Song, X. Zhang, H. Gao, J. Yang and D. Chen, *Journal of Materials Chemistry A*, 2019, **7**, 9708.
- 23 D. Wang, S. Wang and Z. Lu, *International Journal of Energy Research*, 2021, **45**, 2498.
- 24 L. Wang, M. Peng, J. Chen, T. Hu, K. Yuan and Y. Chen, *Advanced Materials*, 2022, **34**, 2203744.
- 25 Z. Pan, Z. Lu, L. Xu and D. Wang, *Applied Surface Science*, 2020, **510**, 145384.
- 26 C. Zhu, H. Wang, W. Fan, S. Zhai, X. Wang, J. Shi, M. Huang, S. Liu, Z. Li and J. Chen, *Rare Metals*, 2022, **41**, 2505.
- 27 X. Deng, J. Li, Z. Shan, J. Sha, L. Ma and N. Zhao, *Journal of Materials Chemistry A*, 2020, **8**, 11617.
- 28 P. Pattananuwat, R. Pornprasertsuk, J. Qin and S. Prasertkaew, *RSC Advances*, 2021, **11**, 35205.
- 29 L. Huang, Y. Xiang, M. Luo, Q. Zhang, H. Zhu, K. Shi and S. Zhu, *Carbon*, 2021, **185**, 1.
- 30 H. Fan, S. Zhou, Q. Chen, G. Gao, Q. Ban, Z. Xu, F. He, G. Hu and X. Hu, *Journal of Power Sources*, 2021, **493**, 229687.
- 31 L. Dong, X. Ma, Y. Li, L. Zhao, W. Liu, J. Cheng, C. Xu, B. Li, Q. Yang and F. Kang,

- Energy Storage Materials*, 2018, **13**, 96.
- 32 X. Shi, H. Zhang, S. Zeng, J. Wang, X. Cao, X. Liu and X. Lu, *ACS Materials Letters*, 2021, **3**, 1291.
- 33 M. Liu, F. Wu, X. Feng, Y. Wang, L. Zheng, X. Li, Y. Li, Y. Gong, Y. Bai and C. Wu, *Science China Materials*, 2023, **66**, 541.
- 34 S. Yang, Y. Cui, G. Yang, S. Zhao, J. Wang, D. Zhao, C. Yang, X. Wang and B. Cao, *Journal of Power Sources*, 2023, **554**, 232347.
- 35 F. Wan, L. Zhang, X. Wang, S. Bi, Z. Niu and J. Chen, *Advanced Functional Materials*, 2018, **28**, 1804975.
- 36 J. Yu, X. Jia, J. Peng, B. Meng, Y. Wei, X. Hou, J. Zhao, N. Yang, K. Xie, D. Chu and L. Li, *ACS Applied Energy Materials*, 2023, **6**, 2728.
- 37 K. Wang, Y. Chen, Y. Liu, H. Zhang, Y. Shen, Z. Pu, H. Qiu and Y. Li, *Journal of Alloys and Compounds*, 2022, **901**, 163588.
- 38 Y. Zhao, H. Hao, T. Song, X. Wang, C. Li and W. Li, *Journal of Power Sources*, 2022, **521**, 230941.
- 39 Y. Zheng, W. Zhao, D. Jia, Y. Liu, L. Cui, D. Wei, R. Zheng and J. Liu, *Chemical Engineering Journal*, 2020, **387**, 124161.
- 40 Q. Wang, S. Wang, X. Guo, L. Ruan, N. Wei, Y. Ma, J. Li, M. Wang, W. Li and W. Zeng, *Advanced Electronic Materials*, 2019, **5**, 1900537.
- 41 J. Zeng, L. Dong, L. Sun, W. Wang, Y. Zhou, L. Wei and X. Guo, *Nano-Micro Letters*, 2020, **13**, 19.
- 42 H. Yu, X. Chen, J. Zhou and H. Wang, *Journal of Materials Science-Materials in Electronics*, 2023, **34**, 675.
- 43 H. Ma, H. Chen, M. Wu, F. Chi, F. Liu, J. Bai, H. Cheng, C. Li and L. Qu, *Angewandte Chemie-International Edition*, 2020, **132**, 14649.
- 44 L. Zhang, D. Wu, G. Wang, Y. Xu, H. Li and X. Yan, *Chinese Chemical Letters*, 2021, **32**, 926.
- 45 A. Amiri, M. Naraghi and A. Polycarpou, *Journal of Energy Chemistry*, 2022, **70**, 480.